Available online at www.sciencedirect.com
ScienceDirect
Journal of Power Sources 163 (2006) 144–150
JOURNAL OF POWER SOURCES
www.elsevier.com/locate/jpowsour

Effect of Fe_2P on the electron conductivity and electrochemical performance of $LiFePO_4$ synthesized by mechanical alloying using Fe^{3+} raw material

Cheol Woo Kim, Jong Suk Park *, Kyung Sub Lee

Department of Materials Science & Engineering, Hanyang University, Seoul 133-791, Republic of Korea

Received 9 August 2005; received in revised form 13 February 2006; accepted 16 February 2006
Available online 29 March 2006

Abstract

$LiFePO_4$ and $LiFePO_4/Fe_2P$ composites have been produced using raw Fe_2O_3 materials by mechanical alloying (MA) and subsequent firing at 900 °C. The $LiFePO_4$ prepared by firing at 900 °C for 30 min showed a maximum discharge capacity of 160 mAh g^{-1} at *C*/20, which is at a higher capacity and improved cell performance compared with the $LiFePO_4$ prepared using for a longer firing times. $LiFePO_4/Fe_2P$ composites have been synthesized by the reduction reaction of phosphate in excess of carbon. By transmission electron microscopy (TEM) and scanning electron microscopy (SEM) it was determined that the $LiFePO_4$ phase was agglomerated with a primary particle size of 40–50 nm around the surface of Fe_2P with particle size of 200 nm. The electronic conductivity of the $LiFePO_4/Fe_2P$ composite increased in proportion with the amount that the Fe_2P phase and discharge capacity increased during the cycling. The sample containing 8% of Fe_2P in $LiFePO_4/Fe_2P$ composite showed a high discharge capacity and rate capability at high current.
© 2006 Elsevier B.V. All rights reserved.

Keywords: $LiFePO_4$; Fe_2P; Olivine-type iron phosphate; Mechanical alloying

1. Introduction

Lithium ion phosphate, $LiFePO_4$, has been considered an attractive alternative cathode material for lithium ion batteries following its description by Padhi et al. [1]. Despite its relatively low costs and environmental benefits, lithium iron phosphate suffers from poor electronic conductivity, which increases the impedance of the electrode and decreases the rate capacity. Various scenarios to overcome these problems have been proposed such as the synthesis of particles to yield well-defined and minimized morphology [2], the coating of the particles with conductive carbon or the co-synthesizing the $LiFePO_4$/C composite [3–6]. These approaches, in spite of excellent electrochemical performance, ultimately led to a loss in energy density due to the electrochemical inertness of the carbon. Unfortunately, the potential low-cost advantage was not materialized by these methods as, although iron components are cheaper than other transition metals, expensive Fe^{2+} precursor compounds were selected as the starting materials in these prior studies. In addition, the conventional solid-state method, which is a general and easy manufacturing process for cathode materials, is needed for several heat treatments and subsequent regrindings to improve the homogeneity of the final products. These repeated firing conditions result in a large particle size.

Chung et al. [7] prepared $LiFePO_4$ doped with a supervalent ion, which is reported to be a semiconductor with p-type conductivities of $\sim 10^{-2}$ S cm^{-1} and an impressive cell performance arising from minority Fe^{3+} hole carriers. But Subramanya Herle et al. [8] have recently argued that a continuous "nano-network" of metal-rich phosphides is responsible for the enhanced electronic conductivity of the doped $LiFePO_4$. Metal phosphates which exhibit a high electron conductivity of about 10^{-1} S cm^{-1} are generated by carbothermal reduction condition at high temperature.

From the above reviews, it is important to develop a synthesis method in which the $LiFePO_4$ is of small particle size while minimizing energy density loss and minimizing costs through the use of cheaper iron precursors in place of divalent iron compounds.

* Corresponding author. Tel.: +82 2 2281 4914; fax: +82 2 2281 4914.
E-mail address: namizs@naver.com (J.S. Park).

0378-7753/$ – see front matter © 2006 Elsevier B.V. All rights reserved.
doi:10.1016/j.jpowsour.2006.02.071

For these reasons, we synthesized $LiFePO_4$ and $LiFePO_4/Fe_2P$ composites by a mechanical alloying (MA) process using trivalent iron. Previously, we reported the effectiveness of the MA process to synthesize the $LiFePO_4$ and $LiFePO_4/C$ composites using both Fe^{2+} and Fe^{3+} raw materials [9,10].

In this study we described the optimum MA and subsequent firing conditions to prepare the $LiFePO_4/Fe_2P$ composite with excellent cell performance, and investigated the effect of Fe_2P on the powder characteristics and electrochemical properties of $LiFePO_4$.

2. Experimental

$LiFePO_4$ was synthesized by mechanical alloying (MA) and subsequent firing at 900 °C for 30 min, 2, 5 and 10 h, respectively, in a tube-type vacuum furnace at a pressure of 10^{-6} Torr using $LiOH{\cdot}H_2O$, Fe_2O_3, $(NH_4)_2H{\cdot}PO_4$ and acetylene black powders, as previously reported [10]. $LiFePO_4/Fe_2P$ composites were prepared by ball-milling the starting materials and with carbon in stoichiometric excess (1, 3, 5, 7, 10 wt.%, respectively), and subsequent firing at 900 °C for 30 min. Each heating rate was 15 °C min^{-1} and cooling rate was 4 °C min^{-1}.

To determine the optimum heat treatment temperature and to evaluate the thermal reactions of the ball milled powders during the synthesis, thermal analyses (TGA and DSC) were carried out for the ball milled powders before heat treatment in argon gas atmosphere. The crystal structures of prepared sample powders were characterized by X-ray diffraction (Rigaku D-MAX 3000) using Cu Kα radiation. The powder morphology and particle size distribution were investigated by a field emission scanning electron microscope (FE-SEM) and a transmission electron microscope (TEM), and a particle size analyzer (PSA). The specific surface area of the powder particles was measured by the Brunauer–Emmett–Teller method (BET), and the electrical conductivity of the prepared samples was measured by the four-point probe method.

The cathodes for electrochemical characterization were fabricated by blending the prepared active material powders with carbon black and polytetrafluoroethylene (PTFE) binder in a weight ratio of 75:20:5. Two-electrode electrochemical cells were assembled with lithium metal foil as the negative electrode, a polypropylene separator and an electrolyte of 1 M $LiPF_6$ in EC:DMC (1:1 in vol.) in an argon-filled glove box. The electrochemical cycle tests were performed using an automatic galvanostatic charge–discharge unit (Maccor series 4000) at various C rates, C/x ($x = 1$, 5, 10, 20) ($1C = 170$ mAh g^{-1}) between 2.5 and 4.3 V at ambient temperature (25 ± 2 °C).

3. Results and discussion

3.1. $LiFePO_4$ prepared by various firing times using Fe^{3+} start materials

In our previous studies [10], it was reported that $LiFePO_4$ was successfully synthesized by MA and subsequent firing at 900 °C using Fe_2O_3 as a raw material for the carbothemal reduction reaction, which was assumed to proceed according to the following equation:

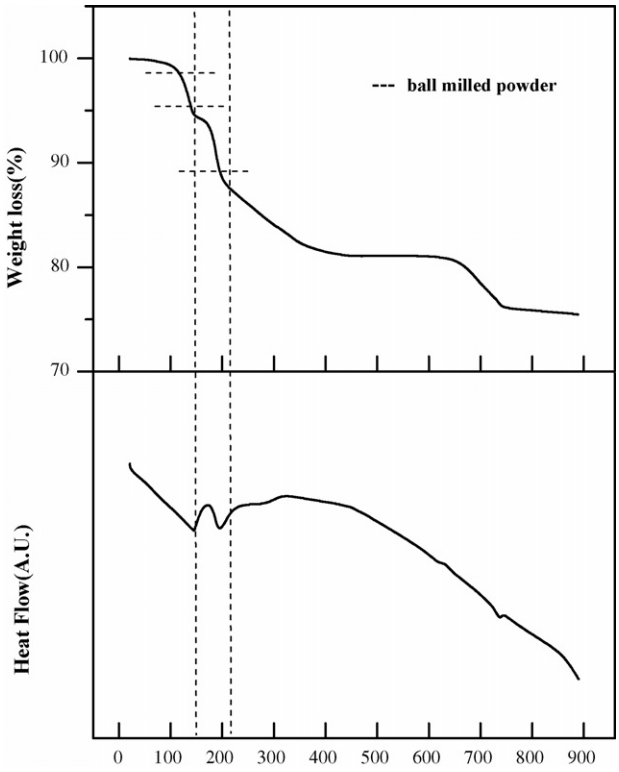

Fig. 1. TG and DSC plots for MA sample in an argon atmosphere.

$$LiOH \cdot H_2O + 0.5(Fe_2O_3) + (NH_4)_2H \cdot PO_4 + 0.5C \rightarrow LiFePO_4 + 3H_2O + 2(NH_3) + 0.5CO \quad (1)$$

Thermal analyses for the ball milled precursors were carried out in order to confirm the above reactions before subsequent firing. The TG and DSC plots for stoichiometric mixtures of the powders by MA are given in Fig. 1. Under the Ar atmosphere, there are various stages of weight loss in the TG plot and both endothermic and exothermic peaks in the DSC plot. In the region from 50 to 150 °C, an initial weight loss of 3.2% and an endothermic peak were observed. This corresponds to the dehydration reaction of $LiOH{\cdot}H_2O$ (i.e. $LiOH{\cdot}H_2O \rightarrow LiOH + H_2O$). As the temperature increased to 210 °C, a second broad endothermic peak and the weight loss of 6.8% appeared in the DSC and the TG plots, respectively. It seems that ammonium hydrogenphosphate was decomposed into ammonia (NH_3) and phosphoric acid (i.e. $(NH_4)_2H{\cdot}PO_4 \rightarrow 2(NH_3) + H_3PO_4$). As the temperature increased above 210 °C up to 480 °C, the TG showed a weight loss of 8% and the DSC plot exhibited a small exothermic peak. This indicated the decomposition of LiOH into lithium and hydroxide ions (i.e. $LiOH \rightarrow Li + OH^-$), and subsequently the powders were transformed to lithium hydrophosphate from H_3PO_4 and water (i.e. $LiOH + H_3PO_4 \rightarrow LiH_2PO_4 + H_2O$). The Fe_2O_3 was reduced to iron with weight loss of 5 wt.% as result of the carbon oxidation reaction in the region of 480–730 °C, which induced olivine $LiFePO_4$ production. Above 730 °C, a continuous weight loss of 1.0% was detected up to 900 °C in the

TG plot. This indicates that single olivine-type $LiFePO_4$ was obtained at 900 °C, which corresponds well with Eq. (1). The above reactions involved may be summarized as:

$$LiOH \cdot H_2O \rightarrow LiOH + H_2O \quad (\text{at } 50\text{–}150\,^\circ\text{C})$$

$$(NH_4)_2H \cdot PO_4 \rightarrow 2(NH)_3 + H_3PO_4 \quad (\text{at } 150\text{–}210\,^\circ\text{C})$$

$$LiOH + H_3PO_4 \rightarrow LiH_2PO_4 + H_2O \quad (\text{at } 210\text{–}480\,^\circ\text{C})$$

$$LiH_2PO_4 + 0.5Fe_2O_3 + 0.5C \rightarrow LiFePO_4 + H_2O + 0.5CO \quad (\text{at } 480\text{–}900\,^\circ\text{C})$$

When the conventional solid-state reaction method was employed to obtain the single phase $LiFePO_4$, a minimum two-step firing and subsequent regrinding procedure was required for good electrochemical performance [2]. The mechanical alloying process, however, required only a one-step heat treatment [9,10].

In this work, the influence of firing time on $LiFePO_4$ prepared by MA and subsequent firing at 900 °C was investigated. The XRD patterns of the $LiFePO_4$ prepared at 900 °C for various firing times (30 min, 2, 5 and 10 h) are presented in Fig. 2. In spite of being subjected to a single heat treatment, each sampled, revealed a single-phase $LiFePO_4$ with a well-ordered olivine structure without impurities. The $LiFePO_4$ composite prepared only for 30 min is expected to maintain smaller particles than samples prepared with longer firing times, giving it the advantages of energy savings and cost reduction. The fact that $LiFePO_4$ synthesis was possible using a short firing time implied that the reaction kinetics of the mixture could be increased by the MA process because of the very intimate grinding of the reactants on the molecular level.

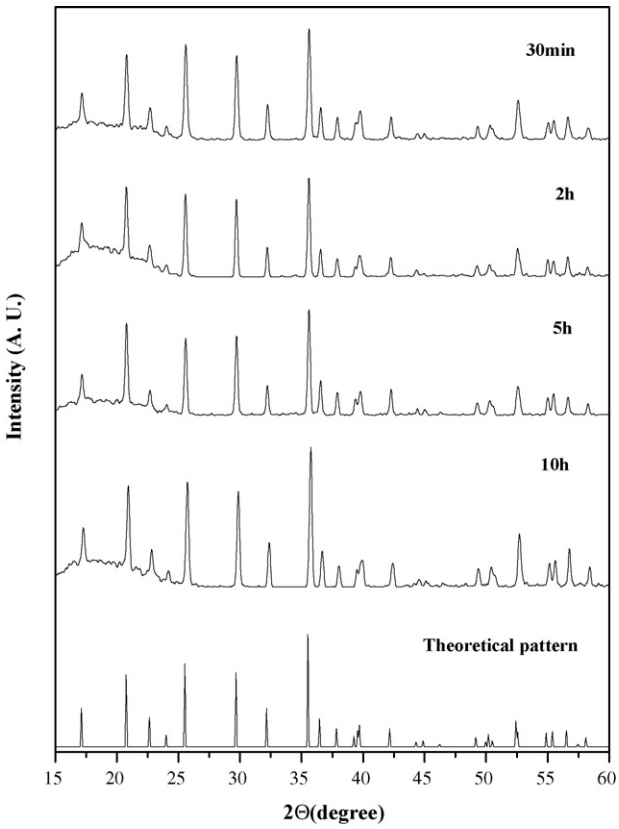

Fig. 2. XRD patterns of $LiFePO_4$ prepared by MA and subsequent firing at 900 °C for various times.

Scanning electron micrographs of $LiFePO_4$ samples fired at 900 °C for 30 min, 2, 5 and 10 h, are shown in Fig. 3. A significant increase in particle size and non-homogeneous morphologies were observed as the firing time increased. The reduced crystal size and particle size are essential for electrical conductivity

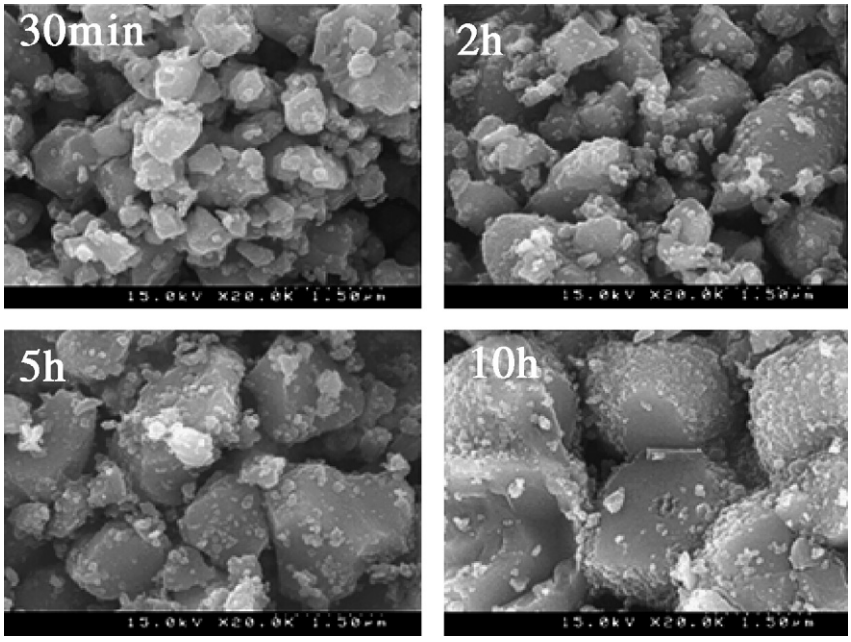

Fig. 3. SEM image of $LiFePO_4$ prepared by MA and subsequent firing at 900 °C for various lengths of time.

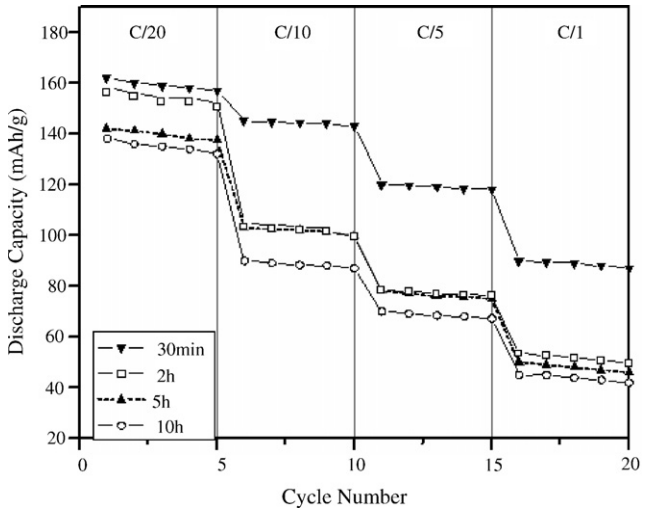

Fig. 4. Discharge capacity as function of cycle number at various rates (*C*/20, *C*/10, *C*/5, *C*/1) using samples fired at 900 °C for various times.

and for the diffusion of the lithium ions during charge–discharge processes [2]. The particle sizes in the sample fired for 30 min ranged from 0.1 to 1 μm, while the sample fired for 10 h contained 3 μm particles. The BET surface areas of the samples (in order of firing times) were 8.7, 7.9, 5.1 and 1.5 $m^2\,g^{-1}$.

A comparison of the discharge capacity as a function of cycle number and firing time is given in Fig. 4. The samples were cycled between 2.5 and 4.3 V at various rates (*C*/20, *C*/10, *C*/5, 1*C*). The discharge capacity of the sample fired for only 30 min was the largest compared to other samples over the entire range of *C* rate, which ranged from 162 mAh g^{-1} at the *C*/20 rate to 90 mAh g^{-1} at the 1*C* rate. By contrast, the discharge capacity of the samples sharply decreased with increasing firing time, particularly at a high current density. This may be due to the agglomeration of the small particles into larger particles during the longer heat treatments. These results correspond well with the study of Yamada et al. [2] who reported that improvements in the conductivity could be achieved by synthesizing small, homogeneously sized powders. However, although the particles were minimized to a sub-micron size, the rate capability of pure the $LiFePO_4$ was still lower than those reported in recent investigations [11–13]. Accordingly, the effect of Fe_2P on $LiFePO_4$ by synthesizing of $LiFePO_4/Fe_2P$ composite was investigated.

3.2. *$LiFePO_4/Fe_2P$ composite prepared by MA*

Chung et al. [7] reported a remarkable increase of eight orders of magnitude in the bulk electronic conductivity of $LiFePO_4$ to a value of 10^{-2} S cm^{-1}. They proposed that a supervalent cation doping makes the $LiFePO_4$ p-type semiconductor with minority Fe^{3+} hole carriers. But, Subramanya Herle et al. [8] recently suggested that the enhanced electronic conductivity of the doped $LiFePO_4$ is due to a continuous "nano-network" of metal-rich phosphides, which arise from carbothermal reduction at high temperature. However, effects of Fe_2P on the synthesized two-phase $LiFePO_4/Fe_2P$ composite have not been reported. It is considered that the electronic conductivity of this material can be increased by the presence or Fe_2P with a conductivity of about 10^{-1} S cm^{-1}.

Here, the $LiFePO_4/Fe_2P$ composite was synthesized by mechanical alloying in order to improve the electrical conductivity. In our previous work [10], the Fe_2P phase was generated by the reduction of phosphate when a stoichiometric excess of carbon (carbon in excess of the stoichiometric amount shown in Eq. (1), reduced the phosphate and generated Fe_2P as follows: $Fe_2O_3 + PO_4 + 7C \rightarrow Fe_2P + 7CO$) was added at 900 °C. The current study controlled the carbon content in the synthesis of the $LiFePO_4/Fe_2P$ composite to optimize the amount of Fe_2P. The starting materials and stoichiometric excess of carbon (1, 3, 5, 7, 10 wt.%, respectively) were ball-milled for 4 h, and subsequently fired at 900 °C for 30 min (denoted as Fe_2P-1, Fe_2P-3, Fe_2P-5, Fe_2P-7 and Fe_2P-10). The XRD patterns for these samples are presented in Fig. 5. In the case of adding 1 wt.% carbon (Fe_2P-1), the olivine $LiFePO_4$ phase was prominent but the impurity of Fe_2P was detected about $2\theta = 40.4°$. The intensities of $LiFePO_4$ phase was reduced and the intensities of iron phosphide of 40.4°, 43° and 47° were dramatically increased with increasing carbon. Relatively Baker et al. reported that residual carbon was detected [16]. Nevertheless, all of our samples were not detected residual carbon. The reason of this result was caused by strong reducing atmosphere in vacuum furnace and formation of Fe_2P.

A qualitative analysis of Fe_2P was performed by the direct comparison method for the integrated intensity of reflection of $LiFePO_4$ and Fe_2P. Qualitative analysis for a particular substance was possible because the intensities of the diffraction lines due to one phase of the mixture depend on the proportion

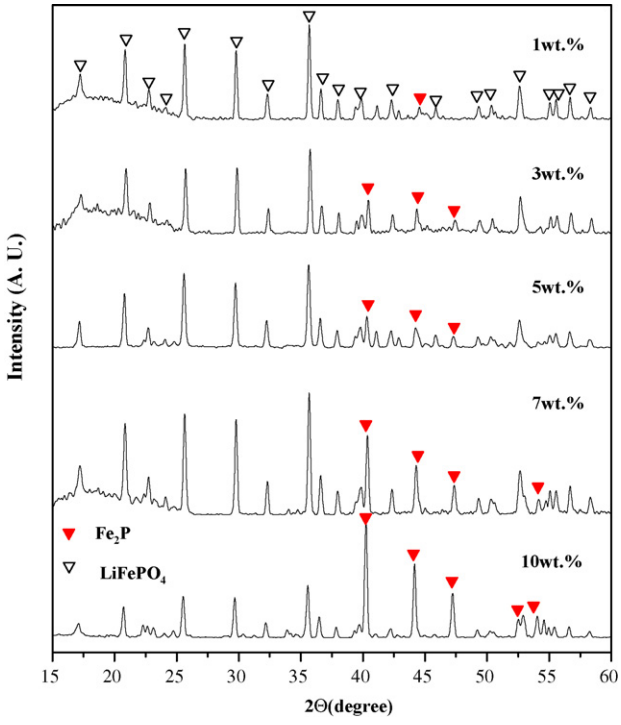

Fig. 5. XRD patterns of the $LiFePO_4/Fe_2P$ composite prepared by adding different amounts of excess carbon (1, 3, 5, 7, 10 wt.%).

Table 1
Powder properties of the $LiFePO_4/Fe_2P$ composites

Sample ID	Synthesis condition	Amount of Fe_2P (%)	Surface area ($m^2\ g^{-1}$)	Particle size (μm)	Electronic conductivity ($S\ cm^{-1}$)
Pure $LiFePO_4$	MA + 900 °C, 30 min	0	8.5	0.1–1	$\sim10^{-7}$
Fe_2P-1	Adding 1 wt.% carbon	2	8.3	0.2–1.5	$\sim10^{-7}$
Fe_2P-3	Adding 3 wt.% carbon	8.3	7.8	0.5–2	$\sim10^{-5}$
Fe_2P-5	Adding 5 wt.% carbon	14.5	7.5	1–2.3	$\sim10^{-4}$
Fe_2P-7	Adding 7 wt.% carbon	20.8	6.5	1.5–3	$\sim10^{-3}$
Fe_2P-10	Adding 10 wt.% carbon	31	5.8	2–4	$\sim10^{-2}$

of that phase in the specimen [14]. The results of the mean particle size, the BET surface area and the electrical conductivity for the $LiFePO_4/Fe_2P$ composite as a function of amount of Fe_2P are summarized in Table 1. It was continuous reaction between carbon depleted and formation of Fe_2P because carbon acting as reducing agent. Therefore, formation of Fe_2P depended on the quantity of excess carbon.

The 1 wt.% carbon sample (Fe_2P-1) had 2% of Fe_2P in the second phase of the $LiFePO_4/Fe_2P$ composite and an electrical conductivity of $10^{-7}\ S\ cm^{-1}$. However, 2 wt.% Fe_2P was not affected to electronic conductivity. In addition electronic conductivity of pure $LiFePO_4$ and Fe_2P-1 was the same even though quantity of carbon was different. By increasing the added carbon, the percentage of Fe_2P was increased and the electrical conductivity of the sample was improved in proportion to the amount of Fe_2P in the $LiFePO_4/Fe_2P$ composite. The Fe_2P-10 sample had a higher conductivity of $10^{-2}\ S\ cm^{-1}$ than $LiCoO_2$ ($\sim10^{-3}\ S\ cm^{-1}$). These results agreed well with the study by Subramanya Herle et al. [8].

Unfortunately, as the amount of Fe_2P increased the average particle size of the $LiFePO_4/Fe_2P$ composite increased and surface area of the composite decreased accordingly. To confirm the increased particle size, transmission electron microscopy (TEM) was used to observe the morphology of the $LiFePO_4/Fe_2P$ com-

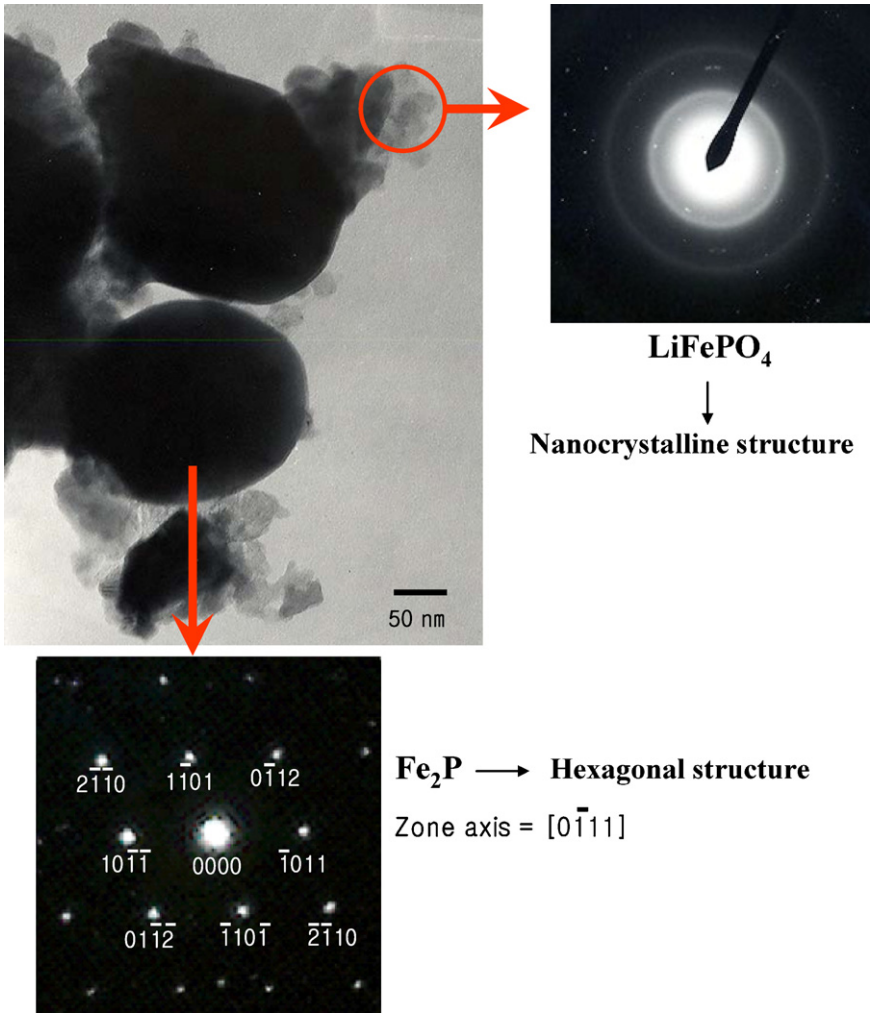

Fig. 6. TEM image of the $LiFePO_4/Fe_2P$ composite.

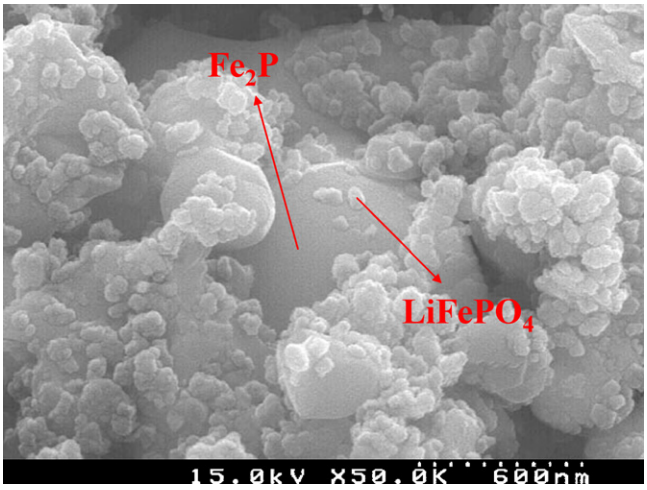

Fig. 7. SEM image of the $LiFePO_4/Fe_2P$ composite.

posite as shown in Fig. 6. The Fe_2P phase appears to be spherical with a crystallite size of about 200 nm, of which the selected area diffraction (SAD) pattern shows a hexagonal structure. The $LiFePO_4$ phase with a primary particle size of 40–50 nm is agglomerated around the surface of the Fe_2P phase, and the corresponding ring type SAD pattern reveals the random and very fine structure of the nanocrystalline grains. In Fig. 7, the SEM image of the $LiFePO_4/Fe_2P$ composite also shows that the fine $LiFePO_4$ particles are dispersed on the surface of the relatively large Fe_2P particles size as also observed in the TEM images. This confirmed that the increase in the average particle size of the $LiFePO_4/Fe_2P$ composite was due to the large particle size of the Fe_2P phase.

3.3. Electrochemical properties of $LiFePO_4/Fe_2P$

Fig. 8 shows the discharge capacity of $LiFePO_4/Fe_2P$ as a function of amount of Fe_2P at *C*/20 and *C*/1 current rates. The discharge capacity of pure $LiFePO_4$ was 162 mAh g^{-1} which was the highest values for all of the samples at the *C*/20 rate. The discharge capacity, however, decreased with increasing the

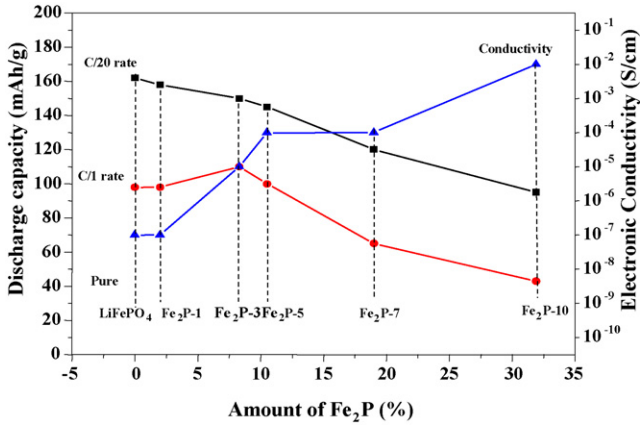

Fig. 8. Electronic conductivity of $LiFePO_4/Fe_2P$ composite as function of Fe_2P concentration and an initial discharge capacity at *C*/20 and *C*/1 current rate (between 2.5 and 4.3 V).

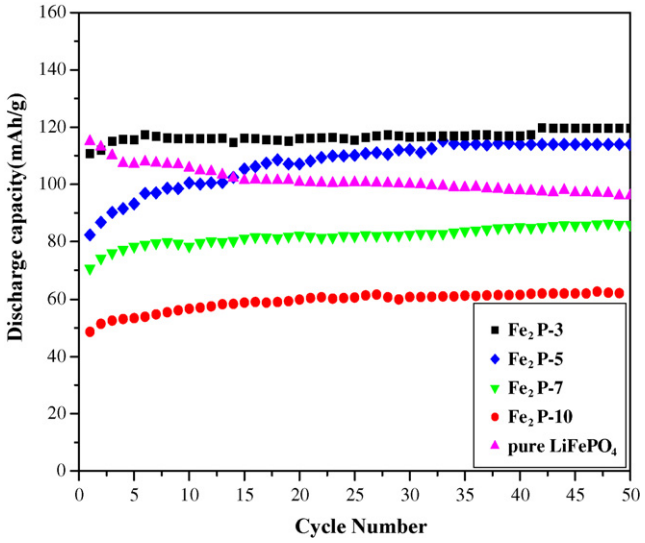

Fig. 9. Cycle life of the $LiFePO_4/Fe_2P$ composites prepared with different carbon concentrations.

amounts of Fe_2P and reached 100 mAh g^{-1} for the Fe_2P-10 sample at the *C*/20 rate. Fe_2P-10 sample contained 31% of Fe_2P which is itself, electrochemically inert and may not have enough lithium ions for intercalation/deintercalation. On the other hand, the Fe_2P-3 sample at the *C*/1 rate contained the largest discharge capacity of 110 mAh g^{-1} while pure $LiFePO_4$ had only a 90 mAh g^{-1} at discharge capacity. It seems that the high rate capability was improved due to an increase in the electronic conductivity. By contrast, the discharge capacity of Fe_2P-10 sample had the lowest capacity with at 50 mAh g^{-1}, even though its electronic conductivity was the highest at 10^{-2} S cm^{-1}. It is considered that the effect of insufficient lithium ions for intercalation/deintercalation was stronger than the effect of increased electrical conductivity. Consequently, the Fe_2P-3 sample containing 8% Fe_2P showed improved electrode performance at high current rate by enhanced electronic conductivity.

The cycle life of $LiFePO_4/Fe_2P$ composites at *C*/5 rate to a cut-off voltage of between 2.5 and 4.3 V is shown in Fig. 9. The discharge capacity of $LiFePO_4/Fe_2P$ composite increased with cycling regardless of amount of Fe_2P present. In the case of the Fe_2P-3 sample, the initial discharge capacity was 113 mAh g^{-1}. After 50 cycles, the discharge capacity was 122 mAh g^{-1}. This behavior is markedly different from the conventional olivine $LiFePO_4$ whose discharge capacity decreases with further cycling [15]. It seems that the lithium ions intercalation/deintercalation reactions into/from an electrode can be disturbed by the Fe_2P phase with relatively great particle at an initial cycling, which causes a loss of the first discharge capacity. As cycling continues, the pathway for lithium diffusion can be stabilize and the reversible reaction of lithium can increase, which results in increased discharge capacity and cycleability. Consequently, it could be concluded that the $LiFePO_4/Fe_2P$ composite enhances the electrical conductivity and improves upon the electrode performance of the olivine $LiFePO_4$ composite.

4. Conclusion

Olivine-type $LiFePO_4$ was successfully synthesized by the MA method and subsequent firing at 900 °C for 30 min using Fe_2O_3. The resulting $LiFePO_4$ had a discharge capacity of 162 mAh g^{-1} and exhibited good electrochemical cycling behavior when compared to $LiFePO_4$ prepared from the conventional solid-state reaction. These improved qualities originated from the uniform distribution of fine particles and the increased specific surface area resulting from the MA process and short firing time. The $LiFePO_4/Fe_2P$ composite was also produced at 900 °C with a stoichiometric excess of carbon by reduction reaction of phosphate resulting in improved electrical conductivity. The sample containing 8% of Fe_2P in the $LiFePO_4/Fe_2P$ composite demonstrated a high discharge capacity and cycleability at a high current rate.

Acknowledgement

This work was supported by the Core Technology Development Program of Ministry of Commerce, Industry and Energy (MOCIE).

References

[1] A.K. Padhi, K.S. Nanjundaswamy, J.B. Goodenough, J. Electrochem. Soc. 144 (1997) 1188.
[2] A. Yamada, S.C. Chung, K. Hinokuma, J. Electrochem. Soc. 148 (2001) A224.
[3] N. Ravet, J.B. Goodenough, S. Besner, M. Simoneau, P. Hovington, Abstract 127 The Electrochemical Society and The Electrochemical Society of Japan Meeting Abstracts, vol. 99-2, Honolulu, HI. October 17–22, 1999.
[4] H. Huang, S.C. Yin, L.F. Nazar, Electrochem. Solid-State Lett. 4 (2001) A170.
[5] Z. Chen, J.R. Dahn, J. Electrochem. Soc. 149 (2002) A1184.
[6] P.P. Prosini, D. Zane, M. Pasquali, Electrochim. Acta 46 (2001) 3517.
[7] S.Y. Chung, J.T. Bloking, Y.M. Chiang, Nat. Mater. 1 (2002) 123.
[8] P. Subramanya Herle, B. Ellils, N. Coombs, L.F. Nazar, Nat. Mater. 3 (2004) 147.
[9] S.J. Kwon, C.W. Kim, W.T. Jeong, K.S. Lee, J. Power Sources 137 (2004) 93.
[10] C.H. Kim, M.H. Lee, W.T. Jeong, K.S. Lee, J. Power Sources 146 (2005) 534–538.
[11] S. Franger, F. Le Cras, C. Bourbon, H. Rouault, Electrochem. Solid-State Lett. 5 (2002) A231.
[12] P.P. Prosini, M. Carewska, S. Scaccia, P. Wisniewski, S. Passerini, M. Pasquali, J. Electrochem. Soc. 149 (2002) A886.
[13] G. Arnold, J. Garche, R. Hemmer, S. Strobele, C. Vogler, M. Wohlfahrt-Mehrens, J. Power Sources 119–121 (2003) 247.
[14] B.D. Cullity, S.R. Stock, Elements of X-Ray Diffraction, third ed., p. 275, 2001 (Chapter 9).
[15] A.S. Andersson, J.O. Tomas, J. Power Sources 97 (2001) 498.
[16] J. Baker, M.Y. Saidi, J.L. Swoyer, Electrochem. Solid-State Lett. 6 (2003) A53.